SSM/I Brightness Temperature Corrections for Incidence Angle Variations

ROLF FUHRHOP AND CLEMENS SIMMER

Institut für Meereskunde an der Universität Kiel, Kiel, Germany

5 July 1994 and 5 June 1995

ABSTRACT

The incidence angles of the SSM/I radiometers on the DMSP satellites vary from satellite to satellite and exhibit variations of up to 1.5° during one orbit. The effects of these variations on the measured brightness temperatures are investigated on the basis of simulated and measured data for oceanic areas. A deviation of 1° from the nominal incidence angle of 53.0° causes brightness temperature changes of up to 2 K depending on surface and atmospheric conditions. Errors of retrieved geophysical parameters on the order of 5%–10% result when the incidence angle variation is not taken into account. This is a common property of most published statistical algorithms. For total precipitable water and cloud liquid water content the error increases with increasing parameter value. For wind speed the error is largest for low wind speed and decreases with increasing wind speed. Due to the slowly varying latitudinal dependence of the incidence angle, these errors do not cancel out when monthly means are computed.

A correction method is developed on the basis of simulated data and tested successfully with measured data. Observed brightness temperature differences between DMSP F10 and F11 are reduced when using corrected data. If diurnal variations of geophysical parameters are investigated, the incidence angle correction is mandatory to obtain useful results, especially for DMSP F10.

1. Introduction

Remote sensing using microwave observations from space is an important diagnostic tool in meteorology. Especially measurements of the Special Sensor Microwave/Imager (SSM/I) onboard the polar-orbiting satellites of the Defense Meteorological Satellite Program (DMSP) are used for the retrieval of geophysical parameters. SSM/I observations have been used in various investigations to estimate hydrological parameters over oceans; for example, total water vapor (e.g., Schluessel and Emery 1990), cloud liquid water (e.g., Karstens et al. 1994), rain (e.g., Adler et al. 1993), and wind speed (e.g., Schluessel and Luthard 1991; Wentz 1992).

In particular over the oceans microwave radiances depend strongly on the incidence angle θ. For this reason most radiometers scan with a fixed incidence angle. This results in the well-known conical scan pattern of microwave radiometers since SMMR (Scanning Multichannel Microwave Radiometer). Elliptical orbits and variations of the satellite orientation lead, however, to variations of θ. This must be taken into account when the resulting radiance variations are on the order or above the radiometer noise. Algorithms based on the direct inversion of the radiative transfer equation (e.g., Wentz 1992; Petty 1994) make allowance for these variations automatically. For SMMR these angle variations were well known and some statistical algorithms did explicitly take θ variations into account (Wilheit and Chang 1980; Prabhakara et al. 1982). Since June 1987 three SSM/I radiometers provide continuous microwave observations from DMSP F8, F10, and F11 satellites. Four frequencies (19, 22, 37, and 85 GHz) with vertical and horizontal polarization, except for 22 GHz, which is vertically polarized only, are measured at a nominal incidence angle of 53.0° (Hollinger 1987). The variations of the incidence angle of the SSM/I radiometers have not been considered by the published statistical algorithms so far.

In this study we investigate the effects of incidence angle variation of the SSM/I radiometers on brightness temperatures (TB) over the ocean. We first analyze the effects of changes in the incidence angle theoretically from the equation of radiative transfer. These results are verified with simulated TB for incidence angles within the expected variability range. For the simulation we use a radiative transfer model, which is described in Karstens et al. (1994) and Simmer (1994). From the simulated TB we developed a correction procedure that gives brightness temperature for oceanic areas adjusted to the nominal incidence angle. Retrievals of total water vapor, cloud liquid water, and wind speed from corrected and uncorrected TB are compared to demonstrate the effects of incidence angle variation.

Corresponding author address: Dr. Rolf Fuhrhop, Institut für Meereskunde an der Universität Kiel, Düsternbrooker Weg 20, D-24105 Kiel, Germany.

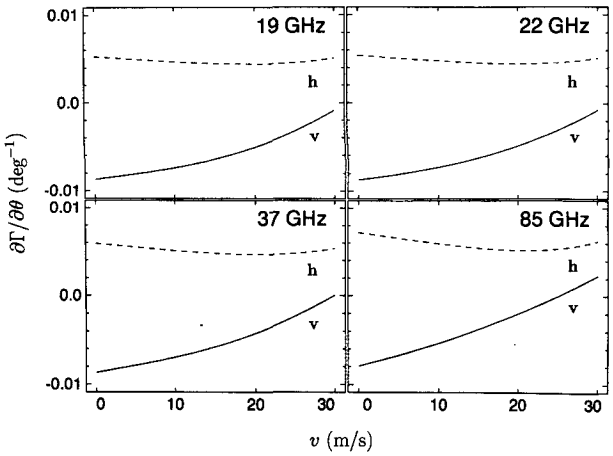

FIG. 1. Change of surface reflectivity with respect to incidence angle ($\partial\Gamma/\partial\theta$) versus wind speed ($v$). Term $\partial\Gamma/\partial\theta$ is calculated as the difference between Γ at 53° and at 52° for vertically (v) and horizontally (h) polarized SSM/I frequencies.

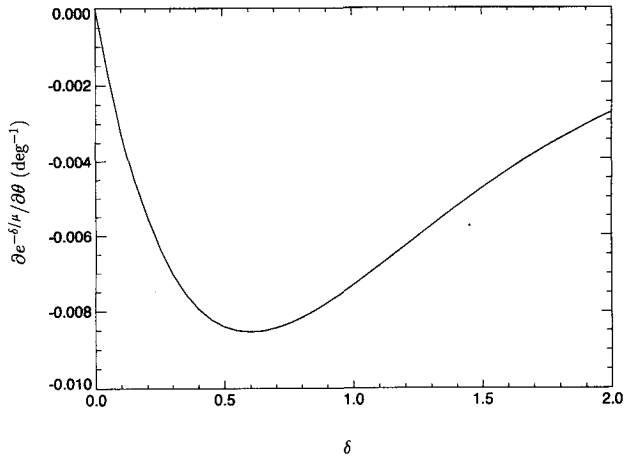

FIG. 2. Change of atmospheric transmission with respect to incidence angle ($\partial e^{-\delta/\mu}/\partial\theta$) versus optical depth ($\delta$) for $\theta = 53°$.

2. Theory

The outgoing microwave radiance at the top of the atmosphere in units of the equivalent blackbody brightness temperature can be adequately described by the solution of the equation of radiative transfer for scatter-free atmospheres and a specular reflecting surface (e.g., Liou 1980):

$$\mathrm{TB} = \underbrace{[1 - \Gamma(\mu)]\,T_s e^{-\delta_a/\mu}}_{\text{(A)}} + \underbrace{\int_0^{\delta_a} T_a(\delta) e^{-\delta/\mu}\,\frac{d\delta}{\mu}}_{\text{(B)}} + \underbrace{\Gamma(\mu) e^{-\delta_a/\mu} \int_0^{\delta_a} T_a(\delta) e^{-(\delta_a-\delta)/\mu}\,\frac{d\delta}{\mu}}_{\text{(C)}} + \underbrace{\Gamma(\mu) T_{\mathrm{sp}} e^{-2\delta_a/\mu}}_{\text{(D)}}, \quad (1)$$

with Γ the surface reflectivity, μ the cosine of the incidence angle θ, δ the nadir optical depth of the atmosphere measured from the top of atmosphere, and δ_a the total nadir optical depth of atmosphere. The surface, air, and space temperatures are denoted by T_s, T_a, and T_{sp}, respectively.

The surface reflectivity $\Gamma(\mu)$ is an essential factor for the surface contribution by emission (term A) and the reflected sky radiation (term C). In our model the effects of surface roughness are parameterized as a function of wind speed and incidence angle using a formulation from Wisler and Hollinger (1977). For horizontal polarization $\partial\Gamma/\partial\theta$ is almost constant (0.005 deg^{-1}), with a small dependence on wind speed and frequency (Fig. 1). For the vertical polarization $\partial\Gamma/\partial\theta$ depends strongly on wind speed with largest values at low wind speeds (−0.01 deg^{-1}) decreasing almost linearly to 0.0 deg^{-1} at 30 m s^{-1}. The atmospheric transmission $e^{-\delta/\mu}$ influences all terms in (1). The change with respect to θ

$$\frac{\partial e^{-\delta/\mu}}{\partial\theta} = -e^{-\delta/\mu}\,\frac{\delta}{\mu^2}\sin\theta \quad (2)$$

is always negative (Fig. 2) because an increase of θ leads to a longer path through the atmosphere. Maximum effects must be expected for optical depths around 0.6, which is about the upper limit for nonraining atmospheres in the low-frequency range (<40 GHz), but a common value for 85 GHz. The effects on TB are in the same range as for the reflectivity

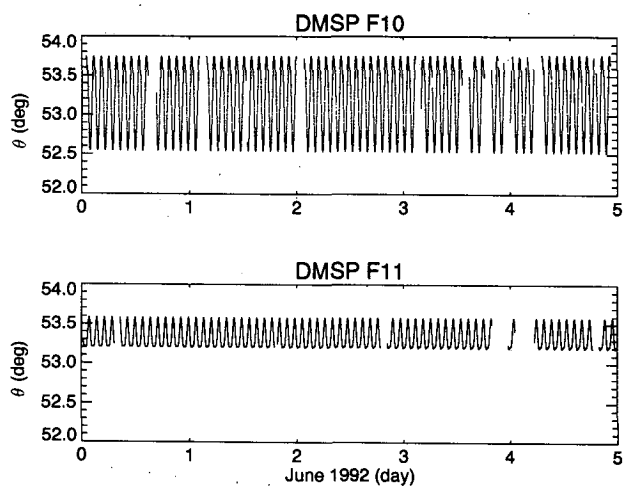

FIG. 3. Time series of incidence angle θ of DMSP F10 and DMSP F11 for 1–5 June 1992. Gaps indicate missing data.

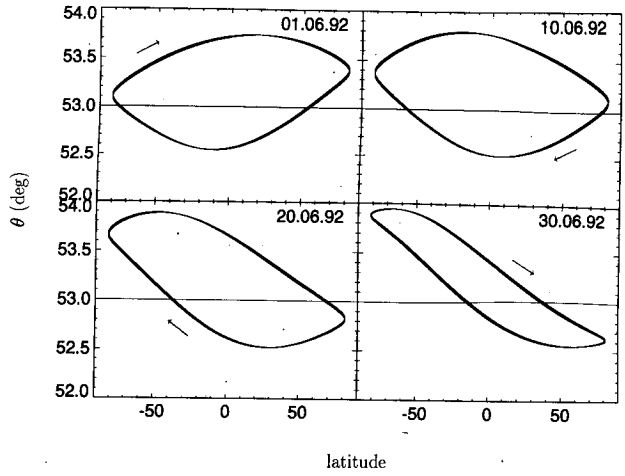

FIG. 4. DMSP F10 incidence angle θ versus latitude for 1, 10, 20, and 30 June 1992; arrow denotes flight direction.

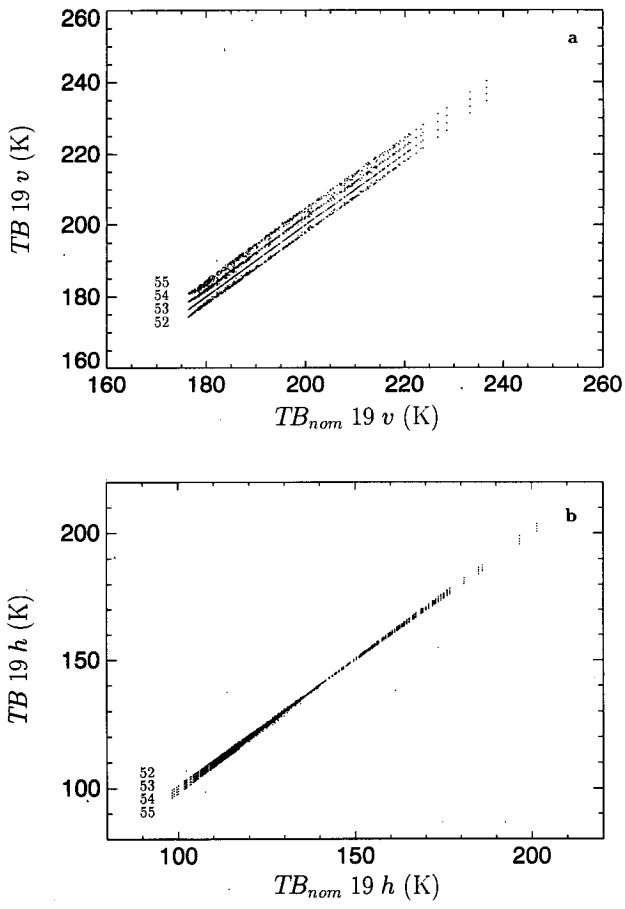

FIG. 5. The 19-GHz brightness temperatures for incidence angles at 52°, 53°, 54°, and 55° versus the nominal brightness temperatures for (a) vertical and (b) horizontal polarization.

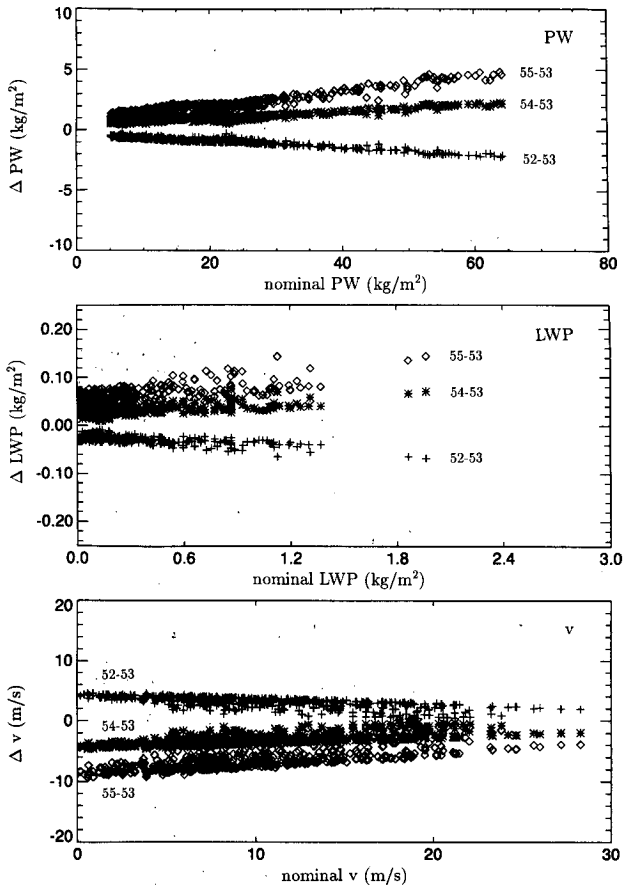

FIG. 6. Differences of precipitable water (PW), liquid water path (LWP), and wind speed (v) between retrievals from simulated brightness temperatures at incidence angles 52° (+), 54° (*), and 55° (◇) and the corresponding retrievals using the nominal brightness temperatures (TB_{nom}), θ = 53°, versus retrieved values from TB_{nom}.

changes discussed above. The total effect of $\partial TB/\partial\theta$ cannot be inferred from this simple analysis. Effects of $\partial\Gamma/\partial\theta$ on the different contributions to TB tend to cancel each other. Model calculations will be used to quantify $\partial TB/\partial\theta$ (chapter 4).

3. Incidence angle variations

In Fig. 3 the incidence angle of the SSM/I radiometers on DMSP F10 (Fig. 3a) and F11 (Fig. 3b) is shown for some days of June 1992. Gaps correspond to missing data periods. The oscillation of θ on DMSP F10 differ from F11 data by the lower amplitude (0.75° and 0.2°) and by a smaller mean value. These oscillations show a strong correlation with the latitudinal position of the subsatellite point. This is more clearly shown in Fig. 4, where we graphed θ for the center pixel of the scan as a function of latitude for 1, 10, 20, and 30 June for SSM/I F10. The line thickness gives an indication of the orbit-to-orbit variation during the day. The latitudinal dependence of θ changes slowly

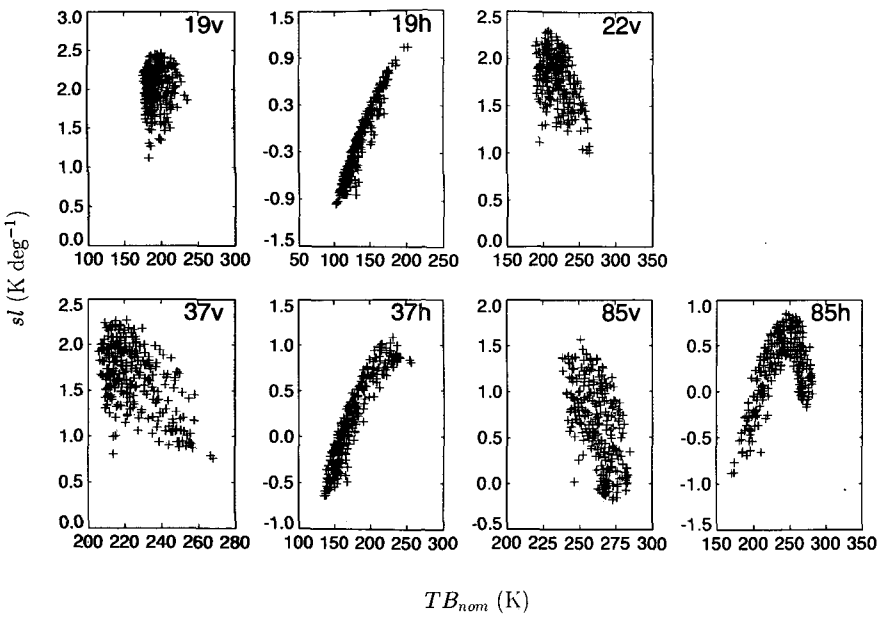

FIG. 7. Change of TB with respect to θ (sl) versus simulated nominal brightness temperatures (TB_{nom}) for SSM/I channels.

with time. At the beginning of the month the angle difference between ascending and descending orbits is largest in the Tropics but becomes smaller and more uniform during the month.

4. Modeling of brightness temperatures

To analyze the total effect of incidence angle variations on TB we simulated TB with our microwave radiative transfer model for about 1000 radiosonde observations over oceanic areas. Cloud liquid water and ice profiles are analyzed based on a method described in Karstens et al. (1994). The simulated TB for the incidence angles of 52°, 53°, 54°, and 55° are shown in Fig. 5 versus the TB for the nominal angle (TB_{nom}) with $\theta = 53°$ for 19 GHz. For the vertically polarized channel (Fig. 5a), the TB for the different incidence angles form nearly parallel lines and $\partial TB/\partial\theta$ is almost independent from TB_{nom}. For the horizontally polarized channel, the lines intersect at about 150 K (Fig. 5b) and $\partial TB/\partial\theta$ depends on TB_{nom}. This feature is also found for the other SSM/I frequencies.

To demonstrate that the TB differences caused by θ variations are crucial for remote sensing of meteorological parameters over oceans, we applied statistical algorithms (see the appendix) for precipitable water (PW) and wind speed (v) developed by Simmer (1994) and for cloud liquid water (LWP) developed by Karstens et al. (1994) to simulated TB for the oceanic environment and various incidence angles. For PW (Fig. 6a) and LWP (Fig. 6b) the differences from the nominal values are 5%–10% for 1° deviation of θ from the nominal angle. For the retrieved wind speed the differences decrease with increasing wind speed and are largest for low wind speeds with errors up to 5 m s^{-1}. From these results it is obvious that a correction of the TB for incidence angle deviations is necessary for statistical algorithms.

5. TB correction for incidence angle variations

To derive a TB correction to compensate for incidence angle variations, we analyzed the functional patterns of TB variations with increasing incidence angle.

TABLE 1. Coefficients a_{ij} to calculate the sl_i from SSM/I TB according to Eq. (4). The corresponding correlation coefficient and standard error of regression is denoted by r and σ, respectively.

Channel	a_0	a_{19v}	a_{19h}	a_{22v}	a_{37v}	a_{37h}	r	σ
19v	−7.586	0.07848	−0.06253	0.007633	0.0	0.006136	0.98	0.054
19h	−6.964	0.0	0.0	0.01499	0.01551	0.0	0.99	0.061
22v	−4.791	0.06859	−0.05930	0.0	0.0	0.006853	0.91	0.112
37v	−6.142	0.06069	−0.05812	0.01731	0.0	0.0	0.98	0.080
37h	−5.578	0.0	−0.02596	0.02358	0.0	0.02314	0.98	0.11

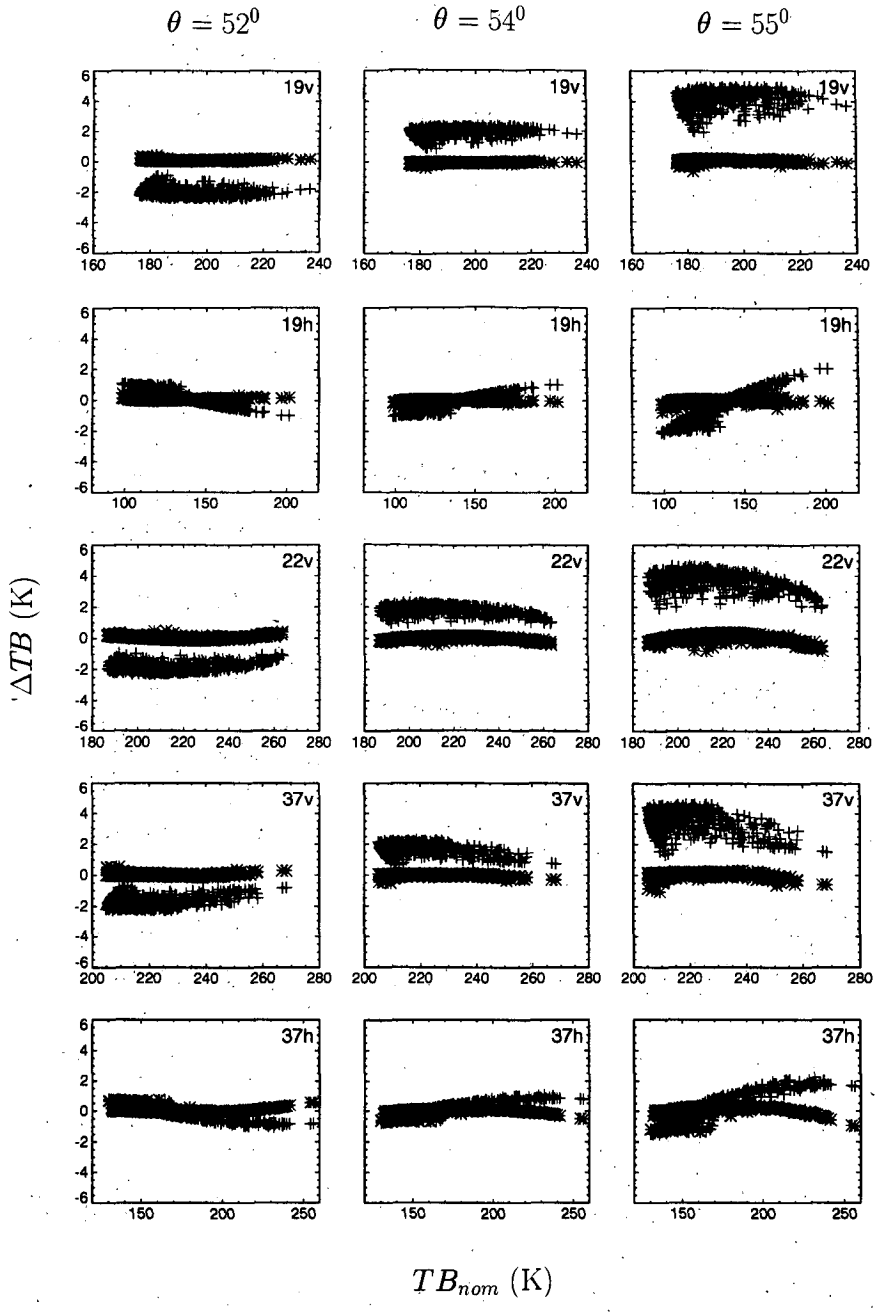

FIG. 8. Deviations of corrected (*) and uncorrected (+) simulated brightness temperatures from nominal brightness temperatures (TB_{nom}) for incidence angles, 52°, 54°, and 55° versus TB_{nom}.

For all SSM/I channels a fairly linear relation exists between TB and the incidence angle deviation $\Delta\theta$ from the nominal value

$$\mathrm{TB}(\theta) = \mathrm{TB}_{\mathrm{nom}} + \mathrm{sl}\Delta\theta, \tag{3}$$

with $\mathrm{sl} = \partial\mathrm{TB}/\partial\theta$. If sl is known we can calculate TB for the nominal angle by inverting (3). A more detailed analysis has shown that sl is fairly independent from θ within the observed incidence angle range but is a function of TB. For the horizontally polarized channels sl is to a first approximation a linear function of $\mathrm{TB}_{\mathrm{nom}}$, but no simple relation exists for the vertically polarized channels (Fig. 7). Term sl depends largely on the state of atmosphere and ocean surface, which in turn determine TB. Hence, we estimate sl from the simulated $\mathrm{TB}_{\mathrm{nom}}$ by multiple regression

$$\mathrm{sl}_i = a_{0i} + \sum_j a_{ij}\mathrm{TB}_{\mathrm{nom}_j}, \tag{4}$$

TABLE 2. Root-mean-square differences of corrected and nominal TB for simulated data with different incidence angles. The bias is always zero. NEΔT denotes the noise equivalent temperature differential for SSM/I F8 (from Hollinger 1989).

Channel	$TB_{52} - TB_{nom}$ rms	$TB_{54} - TB_{nom}$ rms	$TB_{55} - TB_{nom}$ rms	NEΔT
19v	0.06	0.05	0.10	0.45
19h	0.06	0.06	0.12	0.42
22v	0.11	0.11	0.22	0.74
37v	0.08	0.08	0.16	0.37
37h	0.10	0.10	0.21	0.35

where i and j refer to the SSM/I channel numbers (see Table 1). We exclude the 85-GHz channels to avoid errors caused by the much smaller footprint size compared to the other channels.

For measured data TB_{nom} is unknown a priori and we have to combine the sl calculation and TB correction in an iterative manner:

1) the measured TB are taken as a first guess of the TB_{nom};
2) the sl_i are computed according to (4);
3) the TB are corrected according to (3);
4) the corrected TB are used to derive new estimates for the sl_i (continue with step 2).

The iteration continues until the changes in sl_i from the last iteration are smaller than 0.01 K deg^{-1} for all channels, which normally takes less than eight steps. When we apply this correction procedure to simulated TB for different incidence angles, the differences between TB and TB_{nom} are largely reduced (Fig. 8). Adding nonlinear terms to (4) did not improve the adjustment. The remaining rms differences increase with incidence angle deviation, but they are much smaller than the noise equivalent temperature differential estimated by Hollinger (1989) (Table 2).

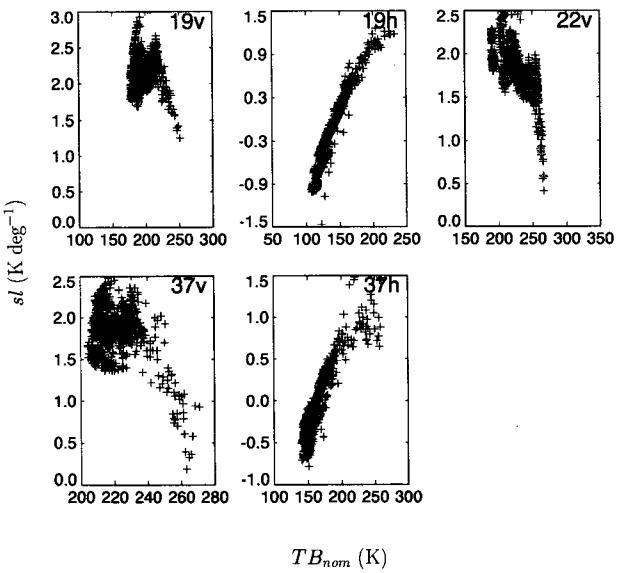

FIG. 9. Calculated sl for the low-frequency SSM/I channels versus the adjusted brightness temperatures for DMSP F10 orbit 7844, 1 June 1992.

6. Results

We applied our TB adjustment procedure to TB measured from the F10 and F11 satellites. The correction for F11 data is necessary, despite a much smaller variation of the incidence angle, because the mean incidence angle is about 0.4° larger than the nominal angle. Since "true" TB measurements are not available we cannot verify our TB adjustment explicitly. We compared instead the scatter diagrams of sl versus TB_{nom} from measured F10 data (Fig. 9) with the simulation results used for the procedure development (Fig. 7). As for the simulated data we found the typical scatter patterns for vertically and horizontally polarized channels for the measured TB. For the vertically polarized channels the sl_i are nearly independent from the corresponding TB_{nom}, while for the horizontally polarized channels a strong correlation with the corresponding TB_{nom} exists. From the good agreement between the scatter diagrams we conclude that the results of our adjustment procedure are reliable.

a. DMSP F10/F11 brightness temperatures

We computed monthly zonal averages of original and adjusted TB for June 1992 for ascending and descending nodes separately (Figs. 10a,b) from F10 and F11 data. The TB differences (F10 minus F11) are reduced when using the adjusted TB. For zonal means the effect of the adjustment is much stronger for the vertically polarized channels than for the horizontally polarized channels, in agreement with the simulation results (Fig. 8). The sign of TB adjustment for vertically polarized channels depends on incidence angle only; for example, for a incidence angle less than the nominal angle the TB correction is always positive. Thus, a positive correction results also for zonal averages because for a given latitude and orbit node the sign of incidence angle deviation is almost constant. For horizontally polarized channels the sign of TB correction depends also on the TB itself. This leads to positive and negative corrections, even if the incidence angle deviation is constant. For the zonal mean, positive and negative

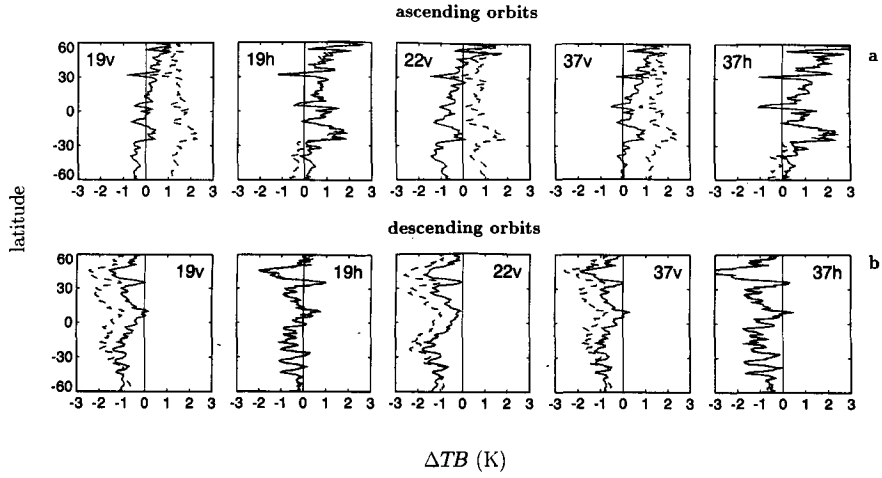

FIG. 10. Monthly zonal average of brightness temperature differences F10 minus F11 for (a) ascending and (b) descending orbits for June 1992. Solid lines represent the difference between F10 and F11 TB, both corrected. Dashed lines represent the difference between F10 uncorrected TB and F11 corrected TB.

corrections tend to cancel each other. However, some differences between F10 and F11 TB remain after the adjustment. The deviations are different for ascending and descending orbits, especially for the horizontally polarized channels.

b. *Adjustment effects on meteorological parameters*

To demonstrate the effect of our TB correction on meteorological parameters we calculated the differences (corrected minus uncorrected) for PW, LWP, and v for the June 1992. The differences strongly depend on latitude and on orbit node and are independent from the monthly mean values (not shown). We computed the zonal averages of the differences for each node separately and for both nodes added for F10 and F11 data (Fig. 11). The differences (both nodes added) for the Northern Hemisphere are smaller than for the Southern Hemisphere for this month. Differences in PW calculated from F10 range from 0.1 to -0.5 kg m^{-2} for the zonal means with both orbits added. The effects on LWP (up to 20 g m^{-2}) and v (up to 2.0 m s^{-1}) are much larger, owing to the lower signal of these parameters in the radiation temperature (Ruprecht et al. 1992). The retrieval differences from F11 show a smaller variation with latitude, but they are as large as found for F10 because of the large incidence angle offset. The observed difference patterns originate from the latitudinal dependency of the incidence angle deviation (Fig. 4). Consequently the large incidence angle variation of F10 leads to a wider range of systematic differences compared to F11. From Fig. 4 also follows that the deviation of θ is different for ascending and descending orbits for the time period investigated, imposing spurious differences of the derived parameters for both orbit parts (Fig. 11). So the angle correction becomes crucial when estimating diurnal variations of meteorological parameters by subtracting the retrieved parameter for the ascending node (evening) from that retrieved for descending node (morning). For each parameter we found artificial diurnal variations when using uncorrected TB (Fig. 12). For F10 an artificial diurnal variation of 3 kg m^{-2} of PW will result for the Tropics, while for LWP the variation is about 40 g m^{-2} for almost all latitudes. The diurnal variations for wind speed is up to 3 m s^{-1} using uncorrected data but much smaller for corrected data. For F11 data the diurnal variations show only a small difference between un-

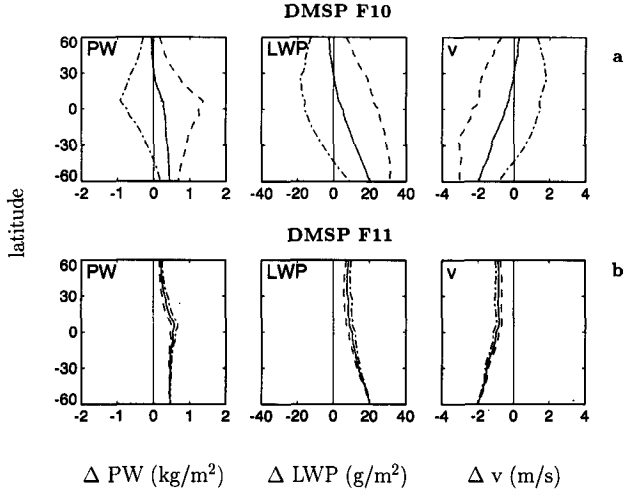

FIG. 11. Monthly zonally averaged differences of precipitable water (PW), liquid water path (LWP), and wind speed (v) between retrievals from corrected and uncorrected brightness temperature for all (solid), ascending-only (dashed), and descending-only (dash–dot) orbits for June 1992, (a) DMSP F10 and (b) DMSP F11.

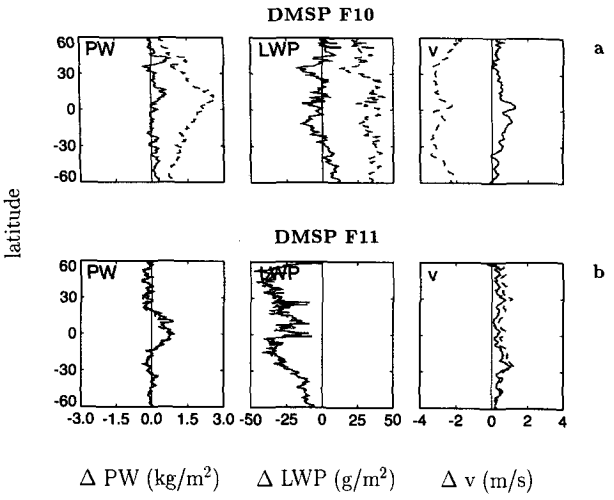

FIG. 12. Monthly zonally averaged diurnal variations of precipitable water (PW), liquid water path (LWP), and wind speed (v) retrieved from corrected (solid) and uncorrected (dashed) brightness temperature for June 1992, (a) DMSP F10 and (b) DMSP F11.

corrected and corrected data. They do not coincide, however, with those derived from F10, especially for LWP and for PW in the Tropics. These differences may be due to different local times of satellite overpasses, but calibration errors are also possible.

7. Summary and discussion

From theoretical considerations it is obvious that TB for SSM/I channels are sensitive to variations of incidence angle. This sensitivity arises from two facts.

(i) The surface reflection (and emission) depends strongly on the incidence angle and the sign of $\partial\Gamma/\partial\theta$ is opposite for vertical and horizontal polarization. For the vertically polarized frequencies $\partial\Gamma/\partial\theta$ is a function of wind speed and is largest for lower wind speeds. For horizontally polarized radiation $\partial\Gamma/\partial\theta$ is less dependent on wind speed. Only a small increase of $\partial\Gamma/\partial\theta$ with increasing frequency is found for both polarizations.

(ii) An incidence angle increase leads to a longer path through the atmosphere and therefore to an increase in effective optical thickness, which depends on frequency.

The effects of θ variations on the surface emission and on the atmospheric transmission tend to cancel each other for vertically polarized frequencies. But they add for horizontally polarized radiation.

The incidence angle deviations of the SSM/I radiometers from the nominal angle show different patterns. The range of θ on F10 is largest ($\approx 1.5°$) and TB variations over 2 K result. The TB corrections for F11 are of the same magnitude but are caused by a large offset from the nominal incidence angle. F8 data for 1987 show a small angle variation that increases slightly over the years with no average offset from the nominal angle. Recently Wentz (1993) reported that the incidence angle of the SSM/I on F8 is biased with 0.336°. Hence the TB adjustment is also necessary for this radiometer. The adjustment of the measured TB to the nominal angle is also necessary, when SSM/I data are used to derive geophysical parameters with algorithms based on the assumption of constant incidence angle (e.g., most statistical methods). Otherwise the effect on retrieved meteorological parameters may be up to 10% for a single observation. Systematic differences between SSM/I retrieved parameters and other methods, especially for wind speed, may at least be partly due to incidence angle variations. The incidence angle variations are correlated with latitude and introduce systematic errors, which will affect investigations of hemispheric structures even on monthly mean basis. The correlation of the incidence angle deviations with orbit position leads to errors when diurnal variations are estimated from the difference between ascending and descending orbits.

For a cross calibration of the F10 and F11 radiometers it is necessary to use the adjusted TB, otherwise systematic errors will be introduced (Fig. 10). The F10/F11 TB differences are probably due to absolute calibration offsets. Scattering due to rain drops and different footprint sizes of the SSM/I channels in conjunction with spatial inhomogeneities of geophysical parameters can lead to errors in sl computation for individual observations. But we believe that this will have negligible effects, at least for zonal averages.

Acknowledgments. This investigation was funded by the Deutsche Forschungsgemeinschaft, Sonderforschungsbereich 133. The radiosonde observations were provided by the Deutscher Wetterdienst, Offenbach, and the Alfred-Wegener-Institut, Bremerhaven.

APPENDIX

Algorithms for Geophysical Parameters

The detailed derivation of the algorithms can be found in Simmer (1994). Here we give the formulation of the algorithms only. The algorithm for precipitable water (PW) is split into three ranges

$$\mathrm{PW} = \begin{cases} \mathrm{PW}_1, & \mathrm{PW}_1 < 15 \\ \mathrm{PW}_2, & \mathrm{PW}_1 \geqslant 25 \\ \mathrm{PW}_3, & \mathrm{PW}_1 \geqslant 15 \quad \text{and} \quad \mathrm{PW}_1 < 25, \end{cases}$$

with

$$\mathrm{PW}_1 = 260.82 - 48.128 \ln(290 - \mathrm{TB}_{22v}) - 0.15718\mathrm{TB}_{37v}$$

$$\mathrm{PW}_2 = 136.03 - 37.673 \ln(280 - \mathrm{TB}_{22v}) + 9.7465 \ln(280 - \mathrm{TB}_{37v})$$

$$\mathrm{PW}_3 = \mathrm{PW}_1 + [(\mathrm{PW}_2 - \mathrm{PW}_1)0.1][(\mathrm{PW}_1 + \mathrm{PW}_2)0.5 - 15.0].$$

TABLE A1. Mean TB deviations between measured SSM/I TB (F8) and the radiative transfer model used to derive the algorithms for geophysical parameters (Simmer 1994).

SSM/I channel	19v	19h	22v	37v	37h
ΔTB	3.3	2.7	2.3	−1.8	−0.9

The surface wind speed v is retrieved by $v = 239.26 + 0.5196TB_{19v} + 0.2062TB_{19h} - 0.2722TB_{22v} - 2.0529TB_{37v} + 0.9279TB_{37h}$. The liquid water path estimation is from Karstens et al. (1994):

$$LWP = 4.299 + 0.3996 \ln(280 - TB_{22v}) - 1.4069 \ln(280 - TB_{37v}).$$

Before these algorithms are applied, the measured TB have to be adjusted in order to remove systematic differences between the model used for algorithm development and the SSM/I radiometers by $TB_{cor} = TB_{meas} + C_m$. The C_m are estimated by a comparison of F8 TB and in situ measurements and are given in Table A1. These adjustments are also used for F10 and F11 data.

A comparison of radiosonde observations and retrievals of PW and v from F8 TB gave an rms error of 2.4 kg m^{-2} for PW and 3.0 m s^{-1} for v. The error of LWP is estimated to 35 g m^{-2}.

REFERENCES

Adler, R. F., A. J. Negri, P. R. Keehn, and I. M. Hakkarinen, 1993: Estimation of monthly rainfall over Japan and surrounding waters from a combination of low-orbit microwave and geosynchronous IR data. *J. Appl. Meteor.*, **32,** 335–356.

Karstens, U., C. Simmer, and E. Ruprecht, 1994: Remote sensing of cloud liquid water. *Meteor. Atmos. Phys.*, **54,** 157–171.

Hollinger, J. P., 1989: DMSP Special Sensor Microwave/Imager calibration/validation. Vol. 1, Tech. Rep., Naval Research Laboratory, Washington, D.C., 182 pp.

——, R. Lo, G. Poe, R. Savage, and J. Peirce, 1987: Special Sensor Microwave/Imager user's guide. Tech. Rep., Naval Research Laboratory, Washington, D.C., 120 pp.

Liou, K. N., 1980: *An Introduction to Atmospheric Radiation.* Academic Press, 392 pp.

Petty, G. W., 1994: Physical retrievals of over-ocean rain rate from Multichannel Microwave Imagery. Part I: Theoretical characteristics of normalized polarization and scattering indices. *Meteor. Atmos. Phys.*, **54,** 79–99.

Prabhakara, C., H. D. Chang, and A. T. Chang, 1982: Remote sensing of precipitable water over the oceans from *Nimbus-7* microwave measurements. *J. Appl. Meteor.*, **21,** 59–68.

Ruprecht, E., R. Fuhrhop, and C. Simmer, 1992: Statistical analysis of the interrelation of the different channel observations of DMSP-SSM/I. *μrad 92 Proceedings of Specialist Meeting on Microwave Radiometry and Remote Sensing Applications,* E. R. Westwater, Ed., NOAA, 276–280.

Schluessel, P., and W. J. Emery, 1990: Atmospheric water vapour over oceans from SSM/I measurements. *Int. J. Remote Sens.*, **11,** 753–766.

——, and H. Luthardt, 1991: Surface wind speeds over the North Sea from Special Sensor Microwave/Imager observations. *J. Geophys. Res.*, **96**(C3), 4845–4853.

Simmer, C., 1994: *Satellitenfernerkundung Hydrologischer Parameter der Atmosphäre mit Mikrowellen.* Verlag, Dr. Kovač, 313 pp.

Wentz, F. J., 1992: Measurement of oceanic wind vector using satellite microwave radiometers. *IEEE Trans. Geosci. Remote Sens.*, **30**(5), 960–972.

——, 1993: User's Manual SSM/I Antenna Temperature Tapes. Revision 2. Tech. Rep. 120193, Remote Sensing Systems, Santa Rosa, CA, 34 pp.

Wilheit, T. T., and A. T. C. Chang, 1980: An algorithm for retrieval of ocean surface and atmospheric parameters from the observations of the scanning multichannel microwave radiometer. *Radio Sci.*, **15**(3), 525–544.

Wisler, M. M., and J. P. Hollinger, 1977: Estimation of marine environmental parameters using microwave radiometric remote sensing systems. Tech. Rep. NRL Memo. Rep. 3661, Naval Research Laboratory, Washington, D.C., 54 pp.